

A SHOCK TUBE STUDY OF THE RADIATIVE COMBINATION OF OXYGEN ATOMS  
BY INVERSE PREDISSOCIATION

B. F. Myers and E. R. Bartle

Space Science Laboratory, General Dynamics/Convair  
San Diego, California, 92112

ABSTRACT

Absolute emission intensity measurements of the radiative combination of oxygen atoms,  $O(^3P)$ , in the temperature range between 2500°K and 3800°K are presented. The emission intensity was recorded simultaneously in six spectral intervals in the wavelength range between 2300Å and 4511Å. The absolute emission intensity was found to be proportional to the square of the oxygen atom concentration and to be characterized by an activation energy of  $28.9 \pm 2.2$  kcal mole<sup>-1</sup>. These results are interpreted in terms of an inverse predissociation mechanism in which the oxygen atoms combine along a repulsive potential energy surface with a transition to the  $B^3\Sigma_u^-$  state of molecular oxygen and a subsequent radiative transition to the ground electronic state of oxygen. The rate constant for the overall radiative combination of oxygen atoms was found to be  $4.3 \times 10^9 \exp(-28900 \pm 2200/RT)$  cm<sup>3</sup> mole<sup>-1</sup> sec<sup>-1</sup> for the wavelength range 2300Å to 5000Å.

I. INTRODUCTION

Measurements on the radiative combination of oxygen atoms,  $O(^3P)$ , in the temperature range between 2500°K and 3800°K are presented. This radiative process was first observed during an investigation<sup>1</sup> on the radiative combination of atomic oxygen and carbon monoxide. In the latter case, it was found that a contribution to the total emission intensity occurred at wavelengths below 4500Å in the presence of oxygen atoms only.

In the present experiments, absolute emission intensity measurements of the radiation resulting from the combination of oxygen atoms were made by shock heating  $O_3 + Ar$  gas mixtures to temperatures in the range cited above and to pressures between 0.5 and 2.0 atm. The emission intensity was recorded simultaneously in six spectral intervals in the wavelength range between 2300Å and 4511Å. The emission intensity behind the shock front at the time of essentially complete ozone decomposition was correlated with the oxygen atom concentrations as determined by numerical calculations.

II. EXPERIMENTAL

The experiments were conducted with the 3 inch, internal diameter shock tube facility and the associated optical system and gas handling system previously employed.<sup>1</sup> For the measurement of the emission intensity of the radiative combination of oxygen atoms, the six slits in the image plane of the spectrograph had the center wavelengths and bandpasses given in Table I. The wavelength values listed have an error of less than 3Å. For detection of incident radiation in the spectral interval between 2300Å and 2500Å, two Dumont 7664 photomultipliers with S-13 spectral response and fused silica windows were employed, and in the spectral interval between 3000Å and 4511Å, four RCA type 1P28, photomultipliers with S-5 spectral response, two of which had quartz windows, were employed. The response of the detector system was linearly related to incident radiation<sup>1</sup> and output signal for each spectral channel was not affected by radiation transmitted in the other channels.<sup>1</sup> The output signals were calibrated in terms of the steradiancy of a calibrated tungsten ribbon filament lamp.<sup>1</sup> The entire optical system was

enclosed in a light tight box which could be flushed with Ar to avoid absorption of the emitted radiation by air.

The gas mixtures of  $O_3$  and Ar were prepared from Matheson Co. supplies of Ar (ultra high purity grade) containing less than 12 ppm of contaminants and from Liquid Carbonic  $O_2$  (electrolytic laboratory grade) containing less than 10 ppm of contaminants. The ozone was synthesized from the oxygen in a static ozone generator.<sup>2</sup> The gas mixtures prepared contained from 1% to 18% of  $O_3$ . The quantitative analysis of the ozone in the prepared gas mixtures was made by a standard titration procedure.<sup>3</sup> For each experiment the test gas mixture was shock heated within three minutes following addition to the shock tube, and a sample of the mixture was withdrawn from the shock tube for ozone analysis one minute before shock heating the mixture.

The  $O_3 + Ar$  mixtures were shock heated to temperatures between 2500°K and 3800°K and pressures between 0.5 and 2.0 atm. At these temperatures and pressures, at least 99% of the ozone had decomposed within 0.1  $\mu$ sec (particle time) behind the incident shock wave to form atomic and molecular oxygen. The concentrations of oxygen atoms and molecules were determined for each experiment by a numerical calculation based on an assumed decomposition mechanism and corresponding elementary reaction rate constants as discussed below. The numerical calculations were made using the Cornell Aeronautical Laboratory normal shock wave computer program.<sup>4,5</sup> The calculations were performed on an IBM 7090-7094 computer.

### III. RESULTS

An oscillogram of the recorded emission intensities is shown in Figure 1. For this experiment, a mixture of 6%  $O_3 + 94%$  Ar was shock heated to an initial temperature of 3048°K and a pressure of 1.41 atm; this temperature and pressure correspond to translational, rotational and vibrational equilibrium of the mixture with frozen chemical reactions. Opposite the beginning of each channel trace in Figure 1, the center wavelength and spectral interval are given in Angstrom units. The shock front arrival is indicated by the sudden rise in the upper trace of Figure 1b which shows the response of a heat resistor gauge mounted in the shock tube wall at the cross section of the radiation measurement. The response time of the detector system is  $\leq 15 \mu$ sec (laboratory time) for all channels except that channel with a center wavelength of 3002Å for which the response time is 20  $\mu$ sec (laboratory time). To obtain the emission intensity immediately after essentially complete ozone decomposition which occurs within 0.1  $\mu$ sec (particle time) of shock front arrival at the observation station, the emission-time profiles are extrapolated practically to zero time. Numerical calculations demonstrate that after the ozone decomposes, the concentrations of atomic and molecular oxygen and the temperature change slowly under the present experimental conditions toward an equilibrium state. For that portion of the emission intensity-time profile following the initial rise in signal, the signal was either constant or linearly increasing or decreasing slowly for 50 to 150  $\mu$ sec (laboratory time), allowing for the noise in the signal; the extrapolation was based on this portion of the trace.

The extrapolated values of the signals near zero time were converted to intensity values for each spectral channel (i) by using the following relation:

$$I_i = \frac{S_i C_i}{[1+R_i]d} \frac{\text{watts}}{\text{str-}\dot{\text{A}}\text{-cm}^2} \quad (1)$$

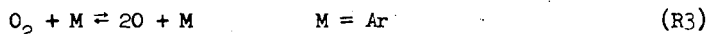
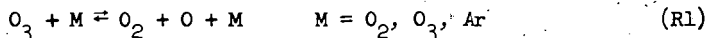
where  $S_i$  is the extrapolated oscillogram signal in volts,  $C_i$ , the calibration factor in watts  $\text{str}^{-1} \dot{\text{A}}^{-1} \text{cm}^{-2} \text{v}^{-1}$ , determined from the measured oscilloscope signal corresponding to the known steradiance of the standardized, tungsten ribbon filament lamp in each wavelength interval of the spectral channels,  $d (= 7.70 \text{ cm})$

the diameter of the shock tube and  $R_1$ , the reflectivity at the center wavelength of channel 1 of the shock tube wall opposite the observation station window which serves as a bounding plane to the optical field. The dependence of the reflectivity on the wavelength which was determined in two independent experiments<sup>6</sup> and the normalization of the intensity with respect to the diameter of the shock tube,  $d$ , have been discussed previously.<sup>1</sup>

The values of  $I_1$  computed as described above, are shown in Table II; also given are the initial conditions, the shock velocity and the calibration factors for each spectral channel.

Contributions to the observed emission intensity from molecular oxygen, argon or impurities in the test gases were examined by shock heating argon and oxygen-argon mixtures to temperatures up to 3600°K. No signal was observed with shock-heated oxygen-argon mixtures until significant decomposition of the molecular oxygen to form oxygen atoms occurred; with shock-heated argon, a signal was observed only in the spectral channel with a center wavelength of 4511Å. This signal was a transient lasting about 50  $\mu$ sec (laboratory time) and was apparently caused by an impurity in the argon or by residual gases in the shock tube. In applying the extrapolation procedure to the data for this channel, the oscillogram trace for  $t(\text{laboratory time}) < 50 \mu\text{sec}$  was disregarded. However, when the extrapolation was made using that portion of the trace for which  $t(\text{laboratory time}) \geq 150 \mu\text{sec}$ , a lower, but not significantly different value of the signal was obtained. The intensities corresponding to the latter signal values are only considered below in connection with Figure 7. This difference could indicate a contribution to the oscillogram trace by the transient signal for  $t(\text{laboratory time}) > 50 \mu\text{sec}$ , although this is difficult to establish because of the signal noise.

For each experiment, the oxygen atom concentration immediately behind the shock front was determined by a numerical calculation based on the following reaction mechanism:



The forward rate constants for these reactions were part of the input data for the computer program<sup>4</sup> while the reverse reaction rate constants were calculated from thermodynamic data and the forward reaction rate constants as part of the computer program. The rate constants for reactions R1 and R2 have been deduced from experiments on the thermal decomposition of ozone at temperatures between 343°K and 383°K in static experiments<sup>7,8</sup> and at temperatures between 689°K and 910°K in shock tube experiments.<sup>9</sup> The relative efficiencies of Ar, O<sub>2</sub> and O<sub>3</sub> in reaction R1 were determined in the low temperature experiments.<sup>7,8</sup> The use of these rate constants at temperatures above 2500°K involves a large extrapolation and recent experiments<sup>10</sup> indicate that the ratio  $k_1/k_2$  is as much as five times smaller than the extrapolated value in the approximate range of temperatures between 1500°K and 2800°K. This conclusion is based on rate constant expressions given in the Arrhenius form.<sup>7,8,9</sup> It will be shown below, however, that this discrepancy is practically resolved for the present experiments by using the rate constant for reaction R1 in the form corresponding to the Hinshelwood-Rice-Ramsperger-Kassel theory of uni-molecular reactions as given by Jones and Davidson<sup>9</sup> and the rate constant for reaction R2 in the collision theory form, i.e.,  $k = AT^{1/2} e^{-E/RT}$ , based on the data of Benson and Axworthy.<sup>7,8</sup> The values of the parameters in these rate constant expressions for reactions R1 and R2 are given in Table III in the group labelled set II; in the group labelled set I, the values of the parameters for the rate constants expressed in the Arrhenius form are given for reactions R1

and R2. The rate constant parameters for the forward direction of R3 are also given in Table III; however, exclusion of the data for R3 from the numerical calculations did not significantly alter the calculated oxygen atom concentration at the time of essentially complete ozone decomposition. To reduce the machine computing time, the calculations were stopped after greater than 99% ozone decomposition and the final oxygen atom concentration was determined by a linear extrapolation based on the concentration of the ozone remaining and on the rate of oxygen atom production per unit ozone concentration in the last machine integration step. Also in making the numerical calculations, the assumption was adopted that the vibrationally excited oxygen, formed in reaction R2,<sup>11</sup> had no effect on the decomposition of ozone. (The chemical relaxation time for ozone decomposition was about 0.1  $\mu$ sec while the vibrational relaxation time for oxygen in the present,<sup>10,12</sup> experiments was between 0.1 and 1.0  $\mu$ sec as estimated from the available data.)

In Table IV, the computed oxygen atom concentrations and the temperatures after ozone decomposition are given. From data in Tables II and IV, it was found that:

$$I_1 = \Gamma_1 (O)^2 \quad (2)$$

where  $I_1$  is the emission intensity in watts  $\text{str}^{-1} \text{\AA}^{-1} \text{cm}^{-3}$  obtained by extrapolating the emission-time profiles on the oscillograms of shock heated  $O_3 + \text{Ar}$  mixtures to the time immediately following shock front arrival at the observation station,  $\Gamma_1$ , a constant for each spectral channel and  $(O)$ , the atomic oxygen concentration in moles  $\text{cm}^{-3}$ . Three examples of data plotted according to equation 2 are shown in Figure 2. The concentration-normalized, absolute emission intensities,  $\Gamma_1$  are functions of the temperature only and the logarithms of  $\Gamma_1$  are found to be linearly related to the reciprocal of the absolute temperature. This is illustrated in Figures 3 and 4 for the six spectral channels employed (see Table I). The lines drawn through the data points are the least squares fits to the data and the vertical bars indicate the standard deviation at the 90% confidence level. The values of  $\Gamma_1$  plotted in these figures were calculated according to equation 2 with oxygen atom concentrations determined from numerical calculations using the rate constants for R1, R2 and R3 given in set II of Table III. When the oxygen atom concentrations were calculated using the rate constants in the Arrhenius form as given in the literature<sup>8,9</sup> and in Table III as set I, the values of  $\Gamma_1$  were found to depend on the initial ozone concentration as shown in Figure 5. In this figure, the lines drawn through the data points are the least squares fits for each initial ozone concentration,  $(O_3)_0$ . In Figure 5, equation 2 is valid for each set of data corresponding to a particular initial ozone concentration. However, as shown in Figures 3 and 4, the dependence of  $\Gamma_1$  on  $(O_3)_0$  can be made insignificant by introducing a reasonable pre-exponential temperature dependence into the rate constant expressions for reactions R1 and R2. For each initial ozone concentration, the data for each spectral channel as shown in Figures 3 and 4 are found not to be significantly different at the 90% confidence level based on the standard deviations determined for the least squares fits to the data at constant  $(O_3)_0$  and  $\lambda_c$ .

From the temperature dependence of  $\Gamma_1$ , as shown in Figures 3 and 4, values of the activation energy  $E_1$ , in the relation

$$\Gamma_1 = A_1 e^{-E_1/RT} \quad (3)$$

were determined for each spectral interval employed; the results are shown in Table V. There is no significant dependence at the 90% confidence level of the activation energy on the wavelength. The average of these activation energies and the corresponding standard deviation are 28.6 and 2.2 kcal mole<sup>-1</sup>, respectively.

Rate constants corresponding to the overall radiative combination of oxygen atoms, i.e., for the process



were calculated at five temperatures and then combined in an Arrhenius expression to obtain the value  $k = 4.3 \times 10^6 \exp(-28900 \pm 2200/RT)$  cm<sup>3</sup> mole<sup>-1</sup> sec<sup>-1</sup> for the wavelength range 2300Å to 5000Å.

#### IV. SUMMARY AND DISCUSSION

Absolute intensity measurements were made of the emitted radiation in the wavelength region between 2300Å and 4511Å; this radiation was observed by shock heating mixtures of ozone and argon to temperatures between 2500°K and 3800°K. The presence of oxygen atoms was necessary to observe this radiation and the absolute emission intensity was found to be proportional only to the square of the oxygen atom concentration at a given temperature. Furthermore, the temperature dependence of the absolute emission intensity normalized with respect to the square of the oxygen atom concentration could be characterized by an activation energy of  $28.9 \pm 2.2$  kcal mole<sup>-1</sup>.

These observations can be rationalized in terms of the potential energy curves for oxygen as shown in Figure 6; the curves presented here were selected from the diagrams of Gilmore.<sup>13</sup> The thermal decomposition of ozone produces ground state oxygen atoms, O(<sup>3</sup>P), which may then combine along several potential energy surfaces. Such a process would be proportional to the square of the oxygen atom concentration, at least. The fact that the radiative process observed has an activation energy of  $28.9 \pm 2.2$  kcal mole<sup>-1</sup> leads to the following suggested mechanism. The ground state oxygen atoms combine along a repulsive potential surface with a subsequent transition to the B<sup>3</sup>Σ<sub>u</sub><sup>-</sup> state of molecular oxygen; the radiative transition from the latter state to the ground state, X<sup>3</sup>Σ<sub>g</sub><sup>-</sup>, then occurs. The vibrational levels of the B<sup>3</sup>Σ<sub>u</sub><sup>-</sup> state from which the transitions originate lie at  $v' \leq 4$ . This conclusion is based on the fact that the energy difference between the  $v' = 4$ ,  $J = 0$  level of the B<sup>3</sup>Σ<sub>u</sub><sup>-</sup> state and the ground state of the oxygen atoms is 30.68 kcal mole<sup>-1</sup> while the upper limit to the experimental activation energy is 31.1 kcal mole<sup>-1</sup> at the 67% confidence level.

The mechanism described is the reverse of a predissociation mechanism suggested<sup>14</sup> to account for observations made during the photolysis of O<sub>2</sub> at 1849Å. In this case, molecular oxygen is excited to the B<sup>3</sup>Σ<sub>u</sub><sup>-</sup> state and predissociates along a repulsive potential curve to yield two oxygen atoms, O(<sup>3</sup>P). Additional photochemical<sup>15</sup> and spectroscopic<sup>16</sup> evidence has been obtained to support this predissociation mechanism.

There are two other mechanisms for the radiative combination of oxygen atoms which are not significant for the shock tube experiments. In one of these, ground electronic state oxygen atoms combine along the potential surfaces leading to the A<sup>3</sup>Σ<sub>u</sub><sup>+</sup>, c<sup>1</sup>Σ<sub>u</sub><sup>-</sup> or C<sup>3</sup>Δ<sub>u</sub> state of O<sub>2</sub> with subsequent radiative transitions to the states, X<sup>3</sup>Σ<sub>g</sub><sup>-</sup> or to b<sup>1</sup>Σ<sub>g</sub><sup>+</sup>. One transition (A<sup>3</sup>Σ<sub>u</sub><sup>+</sup> → X<sup>3</sup>Σ<sub>g</sub><sup>-</sup>, in the wavelength range between 2563Å and 4880Å)<sup>6</sup> and also perhaps several of the other possible transitions have been observed<sup>17,18,19</sup> in flow systems containing atomic oxygen at low pressures and near room temperature. However, this mechanism is inconsistent with the present experimental observations since (a) a near zero activation energy is predicted in contrast to the observed activation energy of 28.9 kcal mole<sup>-1</sup>, and (b) the contribution of the O<sub>2</sub> Herzberg bands to the measured emission intensity is estimated to be less than 3% of the total intensity. The latter conclusion may be demonstrated in two ways. If the value of the room temperature rate constant<sup>18</sup> for the radiative combination of oxygen atoms to give the O<sub>2</sub> Herzberg bands is extrapolated to temperatures greater than 2700°K by assuming a T<sup>-1/2</sup> dependence, this rate constant becomes at least 30 times smaller than the rate constant derived from the present experimental data. Alternatively, the ratio of the emission intensity, I(Schumann-Runge)/I(Herzberg), may be estimated to be greater than 130 on

the basis of a simplified mechanism as shown in Appendix A. In the second mechanism, the oxygen atoms combine along the potential surface of the  $B^3\Sigma_u^-$  state of  $O_2$  after collisional excitation of one of the atoms,  $O(^3P) \rightarrow O(^1D)$ ; the radiative transition  $B^3\Sigma_u^- \rightarrow X^3\Sigma_g^-$  subsequently occurs. This mechanism is also inconsistent with the present experimental observations since (a) an activation energy of about  $45 \text{ kcal mole}^{-1}$  is predicted and this is significantly greater than the observed activation energy, and (b) the spectral intensity distribution resulting from this mechanism is unlikely to result in transitions originating only from  $v' \leq 4$  of the  $B^3\Sigma_u^-$  state of  $O_2$ .

On the assumption that the observed transition is  $B^3\Sigma_u^- \rightarrow X^3\Sigma_g^-$ , a comparison of the experimental and theoretical relative spectral distribution curves indicates that the observed radiative transitions originate primarily from the  $v' = 0$  and 1 levels of the  $B^3\Sigma_u^-$  state. The comparison is shown in Figure 7 for temperatures of  $2632^\circ\text{K}$ ,  $3030^\circ\text{K}$  and  $3571^\circ\text{K}$ ; the experimental data are represented by discrete symbols and the theoretical data are represented, for the sake of clarity, by curves which pass through the data calculated for the experimental spectral intervals which the horizontal bars span. The vertical bars through the symbols represent the standard deviation at the 90% confidence level. In making this graphical comparison, the theoretical relative spectral distribution curves were vertically adjusted so as to coincide with the experimental absolute spectral distribution curve at  $\lambda_c = 3002\text{\AA}$ . The three curves are calculated for transitions originating from  $v' = 0$  and 1, 0, 1 and 2 and 0, 1, 2 and 3 and in this order demonstrate an increasing deviation of the theoretical calculations from the experimental data at wavelengths below  $3000\text{\AA}$ . (The double points at  $\lambda_c = 4511\text{\AA}$  are calculated as described above; the error in these data are too large to permit a comparison with the various theoretical relative spectral distribution curves.) However, the comparison is imprecise and is only employed here to introduce the possibility that the observed radiative transitions may originate primarily from the  $v' = 0$  and 1 levels of the  $B^3\Sigma_u^-$  state. In making the calculations,<sup>21</sup> the assumptions of thermodynamic equilibrium,<sup>20,22,23</sup> of the smeared rotational line model<sup>22,23</sup> and of  $\Delta J = 0$  for all vibration-rotation transitions<sup>20,24</sup> were employed. These assumptions are not strictly valid for use in a comparison with the present experimental data. At the least, the inverse predissociation mechanism predicts a truncation of the population distributions in the vibrational and rotational levels near the crossing level (i.e., near an intersection of the potential curves in a certain low approximation, see ref. 25) which would introduce a perturbation in these distributions. In the converse case of a predissociation mechanism, such a perturbation has been observed<sup>26</sup> and corresponds to that predicted<sup>27</sup> in dissociation processes.

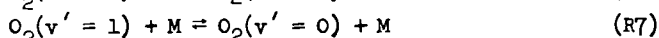
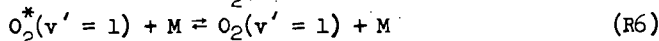
Qualitatively, the statement may be made that calculations which include significant contributions by transitions originating in vibrational levels with  $v' \geq 2$  will result in a predicted intensity greater than observed at wavelengths less than  $3000\text{\AA}$ . This is corroborated by noting that, at  $T = 3030^\circ\text{K}$ , for example, 94% of the observed radiation occurs in the wavelength range between  $2640\text{\AA}$  and  $4400\text{\AA}$ ; this is expected for transitions solely from  $v' = 0$  and 1 to the approximation that the transitions occur only at the classical turning points of the potential curve for the  $B^3\Sigma_u^-$  state. Also, for transitions from the various vibrational levels which contribute to the emission intensity observed in a given spectral interval, the strong influence of transitions from  $v' \geq 2$  on the intensity is indicated, for example, in the wavelength interval between  $2269\text{\AA}$  and  $2331\text{\AA}$  (Channel 1 in Table I) by the relative increase in the Franck-Condon factors; for the levels  $v' = 0, 1, 2, 3$  and  $4$ , the relative magnitudes of the Franck-Condon factors are roughly in the ratios<sup>28</sup>  $1:10:10^2:10^3:5 \times 10^3$ , respectively.

From the experimental absolute spectral distribution curves and the comparison with theoretical relative spectral distribution curves, the tentative conclusion was

reached that radiative transitions originate primarily from the vibrational levels  $v' = 0$  and 1. On the other hand, from the experimental activation energy of  $28.9 \pm 2.2$  kcal mole<sup>-1</sup>, the conclusion is reached that vibrational levels as high as  $v' = 4$  may possibly be occupied by newly formed oxygen molecules in the  $B^3\Sigma_u^-$  state. The relation between these conclusions can be qualitatively understood on the basis of two factors. According to the first factor, there is a preferential transition from one to another potential surface into states with large values of  $J$  (or  $N$ ) and small values of  $v$  ( $< 4$ ), i.e., molecules of  $O_2$  are formed with considerable angular momentum.<sup>29</sup> The second factor accounts for the temperature dependence associated with the vibrational deactivation of the newly formed oxygen molecules; inclusion of this factor in the analysis would result in a value of the energy required to reach the crossing point smaller than the experimental activation energy. These factors will be discussed briefly.

The preferential formation of  $O_2$  in states of large  $J$  and small  $v$  may be understood in terms of the effective potential curves<sup>30</sup> as shown schematically in Figure 8 rather than in terms of the potential curves for a non-rotating molecule such as those shown in Figure 6. The effective potential curves illustrate that for given  $v$  values ( $v = 0$  in Figure 8) the potential curves cross at higher energy values for larger values of  $J$  when the selection rule  $\Delta J = 0$  is taken into consideration.<sup>30</sup> Therefore it is possible to observe an activation energy for molecule formation which is greater than the energy corresponding to the vibrational level occupied ( $v = v'$ ,  $J = 0$ ) as was implied in the conclusions stated above.

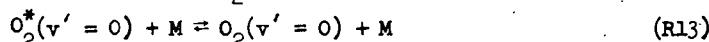
The contribution to the temperature dependence of the absolute emission intensity by the vibrational deactivation of newly formed  $O_2$  molecules can be shown with the aid of the following mechanism:



where  $O_2^*(v' = 1)$  is a newly formed molecule in the  $v' = 1$  level of the  $B^3\Sigma_u^-$  state with the rotational energy corresponding to the crossing level,  $O_2(v' = 0$  or  $1)$ , a molecule with less rotational energy than  $O_2^*(v' = 1)$ , and  $O_2$ , a molecule in the ground electronic state,  $X^3\Sigma_g^-$ . For this mechanism, the following expression for the emission intensity can be derived

$$I = \frac{k_5 k_6}{k_{-5} k_{-6}} k_{10}(0)^2 \left\{ 1 + \frac{k_7}{k_{-7} + k_9 + k_{11} M^{-1}} \right\} \quad (4)$$

when  $k_{-5}$  represents an allowed transition ( $k_{-5} \sim 10^{11}$  sec<sup>-1</sup>),<sup>35</sup> and other rate constants have the values as estimated (see Appendix B). When account is taken of the temperature variation of the bracketed term, the activation energy assigned to  $k_5$  becomes  $\sim 1.5$  kcal mole<sup>-1</sup> smaller than otherwise in accordance with the estimated values of the rate constants. Thus the energy level of the crossing is found on this basis also to be lower than that corresponding to the experimental activation energy. It may be noted that the variation of the bracketed term of Eq. (4) is primarily a result of the temperature coefficient of the vibrational deactivation process represented by  $k_7$ . If, however, the oxygen may be formed in several vibrational levels directly, the effect of vibrational deactivation becomes negligible in the approximations used here. For example, if the following two reactions are added to the above mechanism



then the emission intensity expression becomes

$$I = \left\{ \frac{k_5 k_6}{k_{-5} k_{-6}} + \frac{k_{12} k_{13}}{k_{-12} k_{-13}} \right\} k_{10} (0)^2 \quad (5)$$

and the dependence of  $I$  on  $k_7$  can be neglected.<sup>31</sup> The reverse of this case occurs in predissociation when a breaking-off in successive vibrational levels is observed.<sup>30</sup> In potential curves of the form of those in Figure 8 but including the several vibrational levels of interest, the energy difference of the breaking-off points is found to be large in predissociation. If the reverse of this process were observed in the inverse predissociation mechanism, considered above, it would imply that the observed activation energy is an average over the energy levels corresponding to the several crossing points.

If the radiative transitions observed in the present experiments originate primarily from vibrational levels  $v' = 0$  and 1 of the  $B^3\Sigma_u^-$  state, then predissociation ought to be observed at least in the  $v' = 2$  level. Several spectroscopic experiments<sup>16,32</sup> have led to the observation of predissociation in the  $B^3\Sigma_u^-$  state of oxygen. While interpretation of these experiments does not include predissociation from the  $v' = 2$  level, there is not general agreement<sup>33</sup> that predissociation from the  $v' = 2$  level is excluded. The spectroscopic studies were conducted in absorption and demonstrated predissociation in levels from  $v' = 3$  to  $v' = 12$  with maxima at  $v' = 4$  and 11 and a minimum at  $v' = 9$  in the probability for predissociation. Furthermore, from the investigation<sup>16</sup> of the predissociation at  $v' = 3, 4$  and 5, the transition was found to be allowed and therefore<sup>14,16,32</sup> could be represented as  $B^3\Sigma_u^- \rightarrow {}^3\Pi_u$ . On the basis of calculations, Vanderglice, Mason and Maisch<sup>33</sup> believe the  ${}^3\Pi_u$  curve crosses at the bottom of the  $B^3\Sigma_u^-$  curve and then rises along the left hand branch of the latter curve; the interpretation of the present experiments is in best agreement with this. In postulating this potential curve shape, these authors reject the explanation<sup>16</sup> that the abnormal widths found in absorption for the rotational lines in the 2-0 and 1-0 bands of the Schumann-Runge bands result from a blending of fine structure and imply that predissociation occurs in the  $v' = 0, 1$  and 2 levels. Other potential curve shapes that have been suggested<sup>14,16,32</sup> require a predissociation at  $v' > 3$ ; the above experimental results could only be strictly in agreement with this requirement if a systematic error exists in the relative spectral intensity measurements for  $\lambda \leq 3000\text{\AA}$ . At the present, no such error has been identified. Furthermore, this disagreement would be reduced where the potential curve shape is such that tunneling is important.<sup>32</sup>

The spectral resolution in the present experiments was too small to permit spectroscopic identification of the radiating species. In the oxygen system of potential curves (Figure 6) there are two allowed transitions,  $B^3\Sigma_u^- \rightarrow X^3\Sigma_g^-$ <sup>13</sup> and  ${}^3\Pi_u \rightarrow X^3\Sigma_g^-$ .<sup>32</sup> The latter transition would result in an emission continuum which would shift to lower wavelengths at higher temperatures. Since this is not observed (see Figure 7), the transition  $B^3\Sigma_u^- \rightarrow X^3\Sigma_g^-$  was assumed to be that one detected in the present experiments.

#### APPENDIX A

To estimate the ratio of the emission intensity,  $I$  (Schumann-Runge)/ $I$  (Herzberg), the following simplified mechanism is assumed to apply to both radiative processes:



where  $O_2^*$  is a newly formed molecule in either the  $B^3\Sigma_u^-$  or the  $A^3\Sigma_u^+$ ,  $c^1\Sigma_u^-$  or  $C^3\Delta_u$  states,  $O_2^+$ , a stabilized molecule in one of these states and  $O_2$ , a molecule in the  $X^3\Sigma_g^-$  state. If  $k_2$ ,  $k_{-2}$ , and  $k_3$  are assumed to be identical and larger than  $k_{11} M^{-1}$  for each of the four electronic states, then the ratio of the emission intensities will be:

$$\frac{I_{SR}}{I_H} \approx \left( \frac{k_{4,SR}}{k_{4,H}} \right) \left( \frac{k_{1,SR}}{k_{1,H}} \right) \left( \frac{k_{-1,H}}{k_{-1,SR}} \right) > 130 \quad (A5)$$

where  $k_{4,SR}/k_{4,H} > 10^{5,18,20}$ ;  $(k_{-1,H}/k_{-1,SR}) \sim 10^{13}/10^{11,34,35}$  assuming  $k_{-1}$  to represent an allowed radiationless decomposition<sup>35</sup>; and  $(k_{1,SR}/k_{1,H}) \sim 3 Z_1 10^{-2} e^{-28900/RT/7Z_1}$ , with  $Z_1$ , the collision number,  $3/7$  the ratio of the statistical weights for formation of  $O_2$  in the respective electronic states from which the Schumann-Runge or Herzberg  $O_2$  band transitions originate, and  $10^{-2}$ , the probability of the radiationless transition from the repulsive to the bound state assumed to be equal to the transition probability for the reverse process.<sup>35</sup>

#### APPENDIX B

Estimates of the rate constants for reactions R6 to R11 were made as follows. For  $k_6$  and  $k_{-6}$ , rotational deactivation and activation were assumed to occur at least once in every four collisions so that at 2500°K and 3500°K, the rate constants were  $\geq 1 \times 10^{14}$  and  $1.3 \times 10^{14} \text{ cm}^3 \text{ mole}^{-1} \text{ sec}^{-1}$ , respectively. The rate constant for vibrational deactivation was estimated using the empirical relation of Millikan and White<sup>12</sup> in the following form

$$\log(\rho\tau)^* = (\theta^*/\theta)^{4/3} \log \rho\tau + 8[(\theta^*/\theta)^{4/3} - 1] \quad (B1)$$

where the starred quantities refer to the excited state,  $B^3\Sigma_u^-$  and the unstarred quantities to the ground state,  $X^3\Sigma_g^-$ ;  $\theta$  is the characteristic oscillator temperature and  $\rho\tau$ , the pressure-relaxation time product. The values of  $\tau$  were estimated from data on T-V process for  $O_2-O_2^{12}$  and  $O_2-Ar^{12}$  and from the vibrational relaxation of  $O_2$  by  $O^{10}$  with the following expression:

$$\tau^{-1} = X_{O_2} \tau_{O_2-O_2}^{-1} + X_{O} \tau_{O_2-O}^{-1} + X_{Ar} \tau_{O_2-Ar}^{-1} \quad (B2)$$

where  $X_i$  is the mole fraction of  $i$  and  $\tau_{x-y}$ , the relaxation time of  $x$  in the presence of  $y$ . For the mixtures employed, the average of the estimated values of  $k_7 (= \tau^{-1} M^{-1})$  were  $3 \times 10^{12}$  and  $6 \times 10^{12} \text{ cm}^3 \text{ mole}^{-1} \text{ sec}^{-1}$  at 2500°K and 3500°K, respectively. The activation rate constant,  $k_7$  was estimated from  $k_7 \exp(-1970 \text{ cal mole}^{-1}/RT)$ . The rate constants for electronic deactivation,  $k_8$  and  $k_9$ , were found to be  $4.3 \times 10^{12}$  and  $5.1 \times 10^{12} \text{ cm}^3 \text{ mole}^{-1} \text{ sec}^{-1}$  at 2500°K and 3500°K, respectively on the assumption that one in one hundred collisions was effective for this process. Finally, the radiative rate constants,  $k_{10}$  and  $k_{11}$ , were estimated using the relation

$$k = \tau_R^{-1} = 1.013 \times 10^{-6} \sum q(v', v'') \nu^3(v', v'') \quad (B3)$$

where  $q$  is the Franck-Condon factor for the transition  $v' \rightarrow v''$  and  $\nu$  is the wave number, evaluated at the band head in the approximation employed. For both  $k_{10}$  and  $k_{11}$ ,  $\tau_R^{-1}$  was  $2.7 \times 10^7 \text{ sec}^{-1}$ ; the data of reference 20 were used in this evaluation.

#### VI. ACKNOWLEDGEMENT

The authors are indebted to E. A. Meckstroth for maintaining the operational standard of the shock tube facility and for help in conducting the experiments and to M. R. Schoonover for his assistance in the computer-code preparation and numerical calculations. We thank Mr. K. G. P. Salzman for a critical reading of the manuscript. We gratefully acknowledge support of this work under Contract No. DA-01-021-AMC-12050(Z), ARPA Order 393, Amendment No. 4 through the U. S. Army Missile Command, Redstone, Arsenal, Alabama.

## VII. REFERENCES

1. B. F. Myers and E. R. Bartle, *J. Chem. Phys.*, in press.
2. B. F. Myers, E. R. Bartle, P. R. Erickson and E. A. Meckstroth, *Anal. Chem.* 39, 415 (1967).
3. D. H. Byers and B. E. Saltzman, "Ozone Chemistry and Technology," *Advances in Chemistry Series No. 21*, American Chemical Society, Washington, D. C., 1959, p. 93.
4. L. J. Garr and P. V. Marrone, "Inviscid, Nonequilibrium Flow Behind Bow and Normal Shock Waves, Part II. The IBM 704 Computer Programs," CAL Report No. QM-1626-A-12(II), May 1963.
5. Received by this laboratory through the courtesy of Dr. W. Wurster, Cornell Aeronautical Laboratory, Inc., Buffalo, New York.
6. We are indebted to Dr. J. T. Neu, Space Science Laboratory, General Dynamics/Convair for conducting these experiments.
7. S. W. Benson and A. E. Axworthy, *J. Chem. Phys.* 26, 1718 (1957).
8. S. W. Benson and A. E. Axworthy, *ibid.*, 42, 2614 (1965).
9. W. M. Jones and N. Davidson, *J. Amer. Chem. Soc.* 84, 2868 (1962).
10. J. H. Kiefer and R. W. Lutz, *Symp. Combust. 11th*, Berkeley, 1966, to be published.
11. W. G. McGrath and R. G. W. Norrish, *Proc. Roy. Soc.* A242, 265 (1957).
12. R. C. Millikan and D. R. White, *J. Chem. Phys.* 39, 3209 (1963).
13. F. R. Gilmore, "Potential Energy Curves for N<sub>2</sub>, NO, O<sub>2</sub> and Corresponding Ions," Memorandum RM-4034-1-PR, The Rand Corporation, April 1966. Also published in *J. Quant. Spectry. Radiative Transfer* 5, 369 (1965).
14. P. J. Flory, *J. Chem. Phys.* 4, 23 (1936).
15. D. H. Volman, *ibid.*, 24, 122 (1956).
16. P. K. Carroll, *Astrophysical J.* 129, 794 (1959).
17. H. P. Broida and A. G. Gaydon, *Proc. Roy. Soc.* A222, 181 (1954).
18. R. A. Young and R. L. Sharpless, *J. Chem. Phys.* 39, 1071 (1963).
19. C. A. Barth and M. Patapoff, *Astrophysical J.* 136, 1144 (1962).
20. R. A. Allen, *Avco-Everett Research Report* 236, April, 1966.
21. The method of calculation follows approximately that of reference 20. To obtain the relative spectral distribution curves, the ratios  $(\int_{\Delta\lambda_1} \phi^b d\lambda) / (\int_{\Delta\lambda_3} \phi^b d\lambda)$  were calculated for transitions originating from the levels  $v' = 0$  and 1, 0, 1 and 2 and 0, 1, 2 and 3 which contributed to the emission in the spectral interval  $\Delta\lambda_i$ ;  $\Delta\lambda_i$  represents the wavelength interval corresponding to channel  $i$  ( $i = 1, \dots, 6$ ) in Table I;  $\phi$  is the spectral distribution function.
22. J. C. Keck, J. C. Camm, B. Kivel and T. Wentink, Jr., *Ann. Phys.* 7, 1 (1959).
23. R. W. Patch, W. L. Shackelford and S. S. Penner, *J. Quant. Spectry. Radiative Transfer* 2, 263 (1962).
24. R. A. Allen, *J. Quant. Spectry. Radiative Transfer* 5, 511 (1965).
25. G. Herzberg, "Spectral of Diatomic Molecules," *D. Van Nostrand*, 1950, p. 424.
26. B. P. Levitt, *Trans. Faraday Soc.* 59, 59 (1963).
27. E. E. Nikitin, "Theory of Thermally Induced Gas Phase Reactions," *Indiana University Press*, 1966.
28. These ratios are based on the Franck-Condon factors given in Reference 20.
29. We are indebted to Mr. K. G. P. Sulzmann for bringing this possibility to our attention.
30. G. Herzberg, *op. cit.*, p. 426, 430f.
31. The observed dependence of the absolute emission intensity on  $(0)^2$  (see Figure 2, for example) is, within the experimental error, in accordance with the prediction of the mechanisms represented by either Eq. (5) or (6).
32. P. G. Wilkinson and R. S. Mulliken, *Astrophysical J.* 125, 594 (1947).

33. J. T. Vanderslice, E. A. Mason and W. G. Maisch, *J. Chem. Phys.* **32**, 515 (1960).
34. V. N. Kondrat'ev, "Chemical Kinetics of Gas Reactions," Pergamon Press, 1964, p. 229.
35. G. Herzberg, *op. cit.*, p. 419.

TABLE I: SPECTRAL CHANNEL CENTER WAVELENGTHS AND BANDPASSES

Channel	1	2	3	4	5	6
$\lambda_c, \text{\AA}$	2300	2500	3002	3506	4010	4511
$\Delta\lambda, \text{\AA}$	62	102	200	206	208	202

TABLE III: FORWARD RATE CONSTANTS,  $k^{(a)}$ 

Reaction	Set I			Set II		
	A	n	$E_a$	A	n	$E_a$
1a $O_3 + O_3 \rightarrow O_2 + O + O_3$	$1.4 \times 10^{15}$	0	23.15	$10.91 \times 10^{18}$	-1.25	24.35
1b $O_3 + O_2 \rightarrow 2O_2 + O$	$5.80 \times 10^{14}$	0	23.15	$5.15 \times 10^{18}$	-1.25	24.35
1c $O_3 + Ar \rightarrow O_2 + O + Ar$	$3.76 \times 10^{14}$	0	23.15	$3.12 \times 10^{18}$	-1.25	24.35
2 $O + O_3 \rightarrow 2O_2$	$3.0 \times 10^{13}$	0	5.60	$1.04 \times 10^{12}$	0.50	5.288
3 $O_2 + M \rightarrow 2O + M$	$1.19 \times 10^{21}$	-1.5	118.0	$1.19 \times 10^{21}$	-1.5	118.0

(a)  $k = A T^n e^{-E_a/RT}$ ; units for A,  $\text{cm}^3 \text{mole}^{-1} \text{sec}^{-1}$  or  $\text{cm}^6 \text{mole}^{-2} \text{sec}^{-1}$ , for  $E_a$ , kcal  $\text{mole}^{-1}$ .

TABLE IV: OXYGEN ATOM CONCENTRATIONS AND TEMPERATURES

Run	$(O) \times 10^7$ $\text{mole cm}^{-3}$	$T, ^\circ K$	Run	$(O) \times 10^7$ $\text{mole cm}^{-3}$	$T, ^\circ K$	Run	$(O) \times 10^7$ $\text{mole cm}^{-3}$	$T, ^\circ K$
1014	1.620	2976	1026	0.9073	3130	1041	1.084	3390
1015	1.640	2976	1027	2.218	3097	1042	2.101	3835
1016	2.192	2969	1028	3.360	3164	1043	1.067	3767
1017	2.449	2990	1029	1.500	3259	1044	2.776	3335
1018	0.8171	2939	1030	0.7501	3232	1045	1.422	3728
1019	1.626	2691	1031	2.238	3266	1046	1.365	3530
1020	2.482	2738	1034	1.415	3709	1081	0.3471	3309
1021	0.8370	2718	1035	0.7102	3719	1082	0.5163	3205
1022	1.131	2824	1036	2.119	3698	1083	0.7712	2755
1023	2.186	2841	1039	2.197	3519	1085	0.7963	2494
1024	3.349	2883	1040	1.086	3413	1086	0.6354	2965

TABLE V: THE TEMPERATURE DEPENDENCE OF  $I_0$ 

$\lambda_c, \text{\AA}$	$A_1 \times 10^{-6}, \text{watt str}^{-1} \text{\AA}^{-1} \text{cm}^3 \text{mole}^{-2}$	$E_1, \text{kcal, mole}^{-1}$
2300	1.14	29.8
2500	7.42	27.4
3002	119.2	27.8
3506	89.1	30.4
4010	47.1	31.1
4511	7.38	25.1

TABLE II: SUMMARY OF EXPERIMENTAL DATA

Run	Initial Conditions and Shock Velocity				$I_1 \times 10^9$ , watt str $^{-1}$ Å $^{-1}$ cm $^{-3}$						
	T, °C	P, mm Hg	X <sub>3</sub>	U, mm μsec $^{-1}$	$\lambda_c = 2300\text{Å}$	$\lambda_c = 2500\text{Å}$	$\lambda_c = 3002\text{Å}$	$\lambda_c = 3506\text{Å}$	$\lambda_c = 4010\text{Å}$	$\lambda_c = 4511\text{Å}$	
1014	25.6	18.92	0.060	1.822	---	---	---	12.7	5.39	2.49	
1015	25.0	19.11	0.060	1.822	0.191	1.83	28.0	12.7	6.36	2.92	
1016	24.8	25.54	0.060	1.820	0.313	3.18	48.0	23.0	12.3	4.30	
1017	25.0	28.46	0.060	1.827	0.515	4.32	66.4	31.4	14.0	5.51	
1018	24.7	9.46	0.060	1.811	0.0441	0.442	6.06	3.32	1.47	---	
1019	24.7	20.34	0.060	1.719	0.149	1.285	20.3	8.64	3.85	1.895	
1020	24.5	30.62	0.060	1.736	0.307	3.03	46.5	22.4	10.76	0.516	
1021	24.4	10.16	0.060	1.731	0.0284	0.321	4.94	2.19	0.960	---	
1022	24.7	8.51	0.120	1.799	0.0641	0.735	10.5	5.25	2.88	---	
1023	24.7	16.92	0.120	1.797	0.302	2.91	36.8	17.04	10.2	4.56	
1024	24.6	25.51	0.120	1.813	0.695	6.80	110.2	47.5	25.0	8.94	
1026	24.6	6.17	0.120	1.910	0.066	0.683	9.65	5.03	2.27	1.20	
1027	24.5	15.45	0.120	1.900	0.362	4.46	59.5	27.8	13.04	5.85	
1028	24.5	23.31	0.120	1.924	1.235	11.05	157.0	69.6	33.5	13.76	
1029	24.4	16.60	0.060	1.919	0.277	2.49	36.6	19.4	9.26	3.26	
1030	24.7	8.27	0.060	1.910	0.054	0.564	8.89	4.9	2.06	4.14	
1031	24.8	24.80	0.060	1.921	0.632	5.43	86.0	41.5	18.8	7.91	
1034	24.6	14.91	0.060	2.060	0.429	3.70	30.8	30.8	13.85	4.81	
1035	24.5	7.44	0.060	2.063	0.117	0.905	14.6	7.90	36.8	---	
1036	24.5	22.34	0.060	2.057	0.855	8.15	129.0	69.8	33.3	11.2	
1039	24.8	14.08	0.120	2.052	0.606	6.43	102.1	51.4	33.7	---	
1040	24.5	7.02	0.120	2.018	0.165	1.65	26.1	12.0	5.55	2.06	
1041	25.1	7.05	0.120	2.010	1.64	1.64	23.3	12.3	5.49	2.24	
1042	25.7	12.93	0.120	2.156	1.01	10.0	161.0	75.0	37.6	---	
1043	24.8	6.56	0.120	2.136	0.273	2.34	33.4	18.4	8.51	3.78	
1044	24.4	14.40	0.180	2.010	0.944	8.55	128.8	65.9	26.6	---	
1045	24.5	6.64	0.180	2.159	0.378	3.47	57.2	29.6	14.1	---	
1046	24.9	6.67	0.180	2.088	0.296	2.65	39.5	21.4	9.64	4.30	
1081	24.3	17.67	0.0105	1.864	---	---	1.96	1.05	---	---	
1082	24.2	26.42	0.0105	1.833	---	---	3.83	2.00	---	---	
1083	24.1	40.79	0.0105	1.688	---	---	4.54	2.14	---	---	
1085	23.7	45.93	0.0100	1.597	---	---	3.05	1.36	---	---	
1086	23.4	34.55	0.0100	1.756	---	---	4.29	2.25	---	---	

Calibration factors,  $C \times 10^7$ , watts str $^{-1}$  Å $^{-1}$  cm $^{-2}$  v $^{-1}$ 

15.82

6.81

0.3485

0.0185

0.00303

1.97

0.3485

0.0185

0.00303

1.97

0.3485

0.0185

15.82

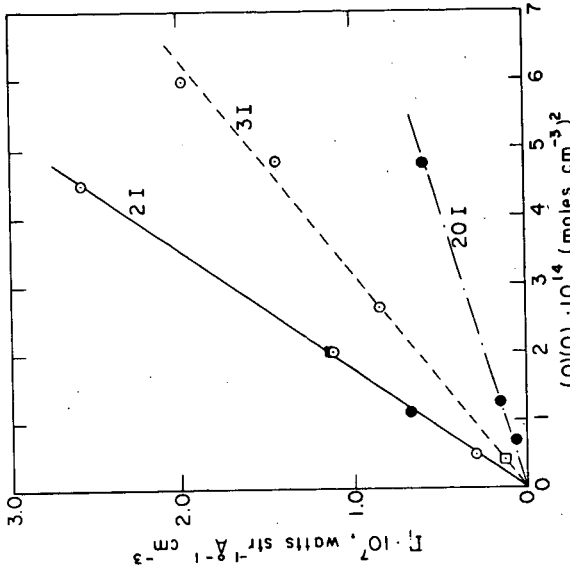


FIGURE 21 ABSOLUTE EMISSION INTENSITY VS.  $(O)^2$ . For  $\lambda = 3506\text{\AA}$ ,  $2096 \leq T^{\circ}K \leq 3726$ ; for  $\lambda = 3002\text{\AA}$ ,  $2965 \leq T^{\circ}K \leq 2990$ ; for  $\lambda = 2900\text{\AA}$ ,  $2716 \leq T^{\circ}K \leq 2641$ . For all curves,  $(O)$  is represented by  $\square$  for 1%,  $\circ$  for 5%,  $\bullet$  for 12% and  $\blacksquare$  for 18%. Each datum on the figure is selected from the results of a different shock tube experiment.

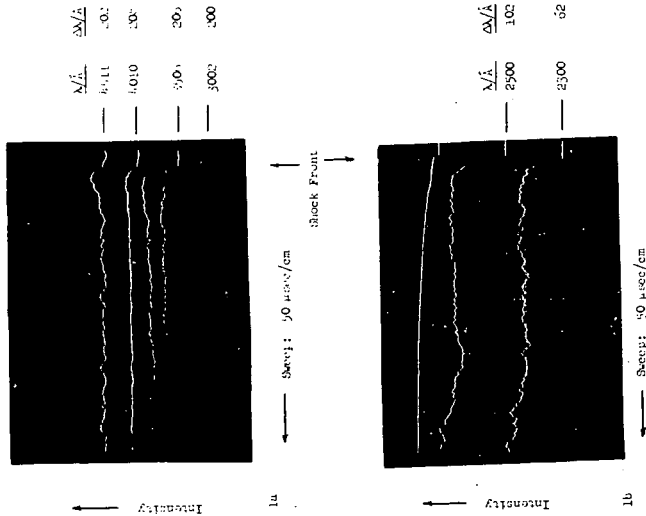


FIGURE 1: INTENSITY TIME OSCILLOGRAM. Oscillogram of the emission behind an incident shock wave traveling through a mixture of 5%  $O_2$  + 95% Ar. Run 1015.

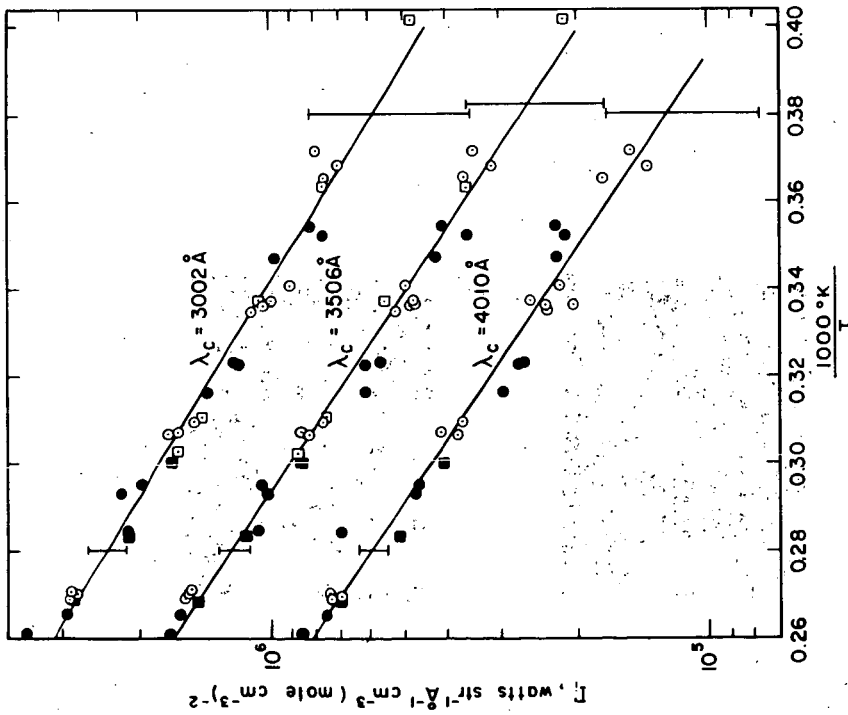


FIGURE 3:  $\log I_\lambda$  vs.  $10000/\lambda T$ . For  $(O_2)_0 = 1\%$ , the data are represented by  $\square$  for  $(O_2)_0 = 6\%$ , by  $\circ$  for  $(O_2)_0 = 12\%$ , by  $\bullet$  and for  $(O_2)_0 = 18\%$  by  $\circ$ . The solid lines are least squares fits to the data and the vertical bars indicate the standard deviation at the 90% confidence level.

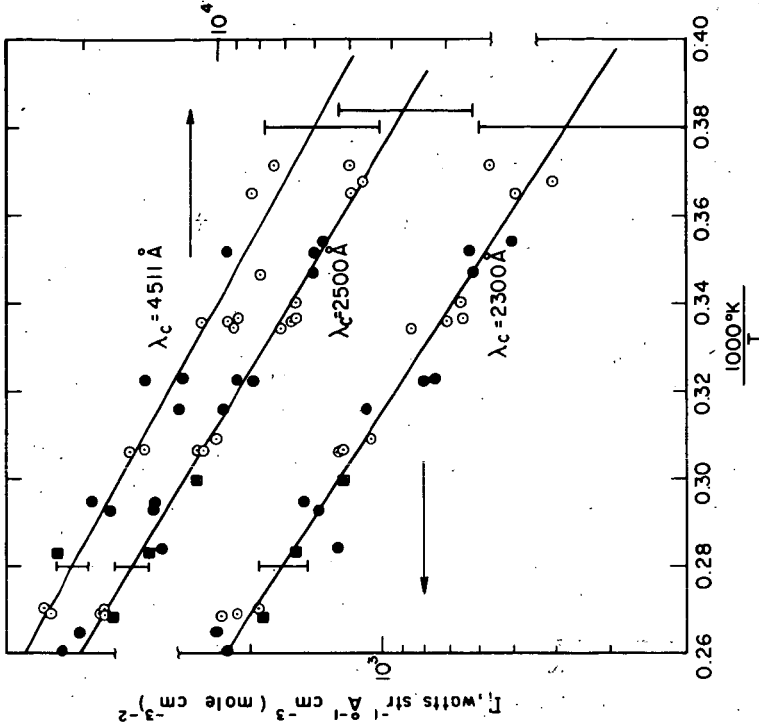


FIGURE 4:  $\log I_\lambda$  vs.  $10000/\lambda T$ . For  $(O_2)_0 = 1\%$ , the data are represented by  $\square$  for  $(O_2)_0 = 6\%$ , by  $\circ$  for  $(O_2)_0 = 12\%$ , by  $\bullet$  and for  $(O_2)_0 = 18\%$  by  $\circ$ . The solid lines are least squares fits to the data and the vertical bars indicate the standard deviation at the 90% confidence level.

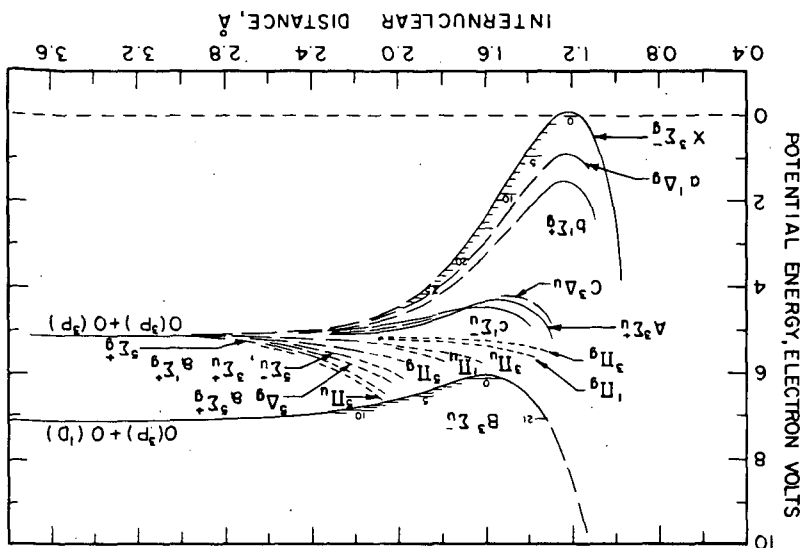


FIGURE 6: POTENTIAL ENERGY CURVES FOR O<sub>2</sub> AFTER GILMORE.<sup>13</sup>

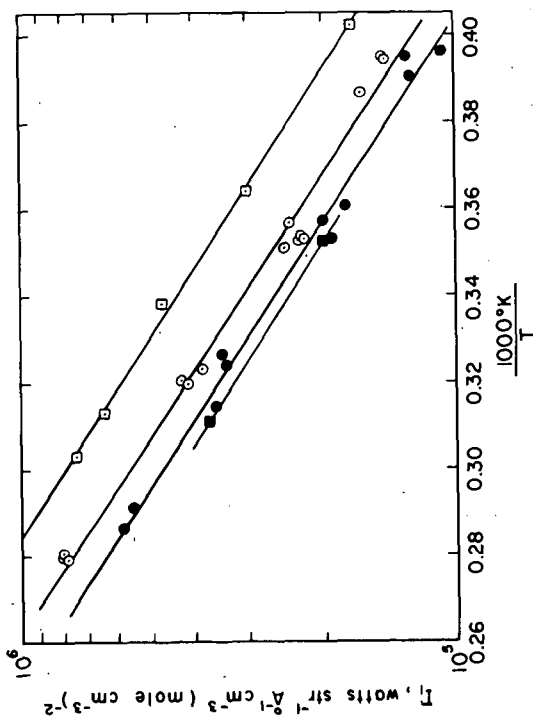


FIGURE 5: LOG I<sub>1</sub> VS 1000°/T. For λ<sub>0</sub> = 3500 Å; curve □ - 1% = (0.3)%; curve ○ - 0% (0.1); curve ● - 1% = (0.1); curve ▽ - 0% (0.1). The solid curves are least squares fits to the data points for each initial ozone concentration.

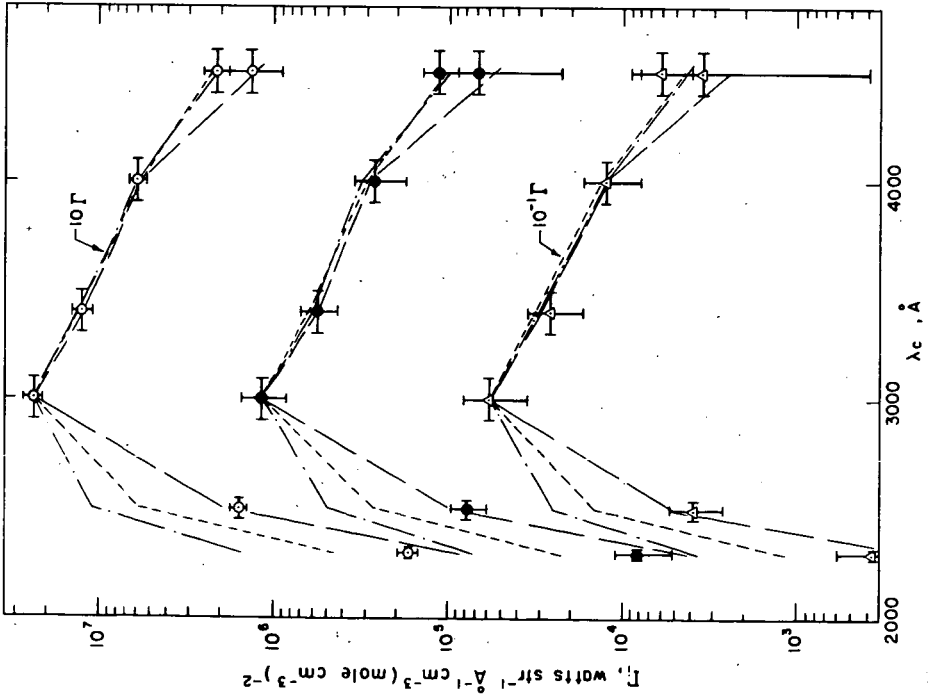


FIGURE 7: ABSOLUTE EMISSION INTENSITY SPECTRAL DISTRIBUTION CURVES.

The experimental data points are represented by  $\odot$  for 3571°K, by  $\bullet$  for 3030°K and by  $\Delta$  for 2532°K. The vertical bar represent the standard deviation at the 90% confidence level and the horizontal bar represent the spectral interval over which the data are average values. The theoretical relative intensity distribution is represented for each temperature by three curves drawn through the points calculated for the  $v=0, 1, 2$  states and the rotational levels indicated by the set of points has been vertically displaced for clarity with the experimental absolute emission intensity values.  $\lambda_c = 3002\text{Å}$  for each temperature. Contributions to the calculated relative intensity from various vibrational levels of the  $B^2\Sigma_u^+$  state have been included as indicated by the legend  $\text{---}$ ,  $v=0, 1, 2$ ;  $\text{---}$ ,  $v=0, 1, 2$ ;  $\text{---}$ ,  $v=0, 1, 2, 3$ . Note that the data sets at the three temperatures have been artificially separated by the factors indicated to improve the clarity of presentation.

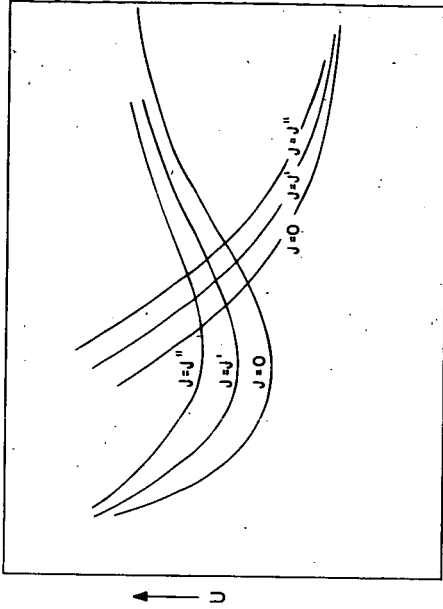


FIGURE 8: EFFECTIVE POTENTIAL CURVES (schematic diagram). The potential energy  $U$  is plotted versus the internuclear distance  $r$  for  $v=0$  and for several rotational levels with  $J' > J'' > J$  and spin splitting neglected.